3D Source Reconstruction Using Coded Aperture Gamma-Ray Imaging

A. Laminack,[1] K. P. Ziock,[2] J. Daughhetee,[2] P. Gibbs,[2] K. Schmitt,[2] and V. Nwadeyi[3]

[1]*National Security Sciences Division, Oak Ridge National Laboratory, Oak Ridge, TN 37831, USA*
[2]*Physics Division, Oak Ridge National Laboratory, Oak Ridge, TN 37831, USA*
[3]*Savannah River National Laboratory*

(Dated: May 12, 2023)

Recent measurements with coded-aperture imagers demonstrate material mass determination in a holdup setting to an accuracy within a few percent. This capability is of particular interest to the Surplus Plutonium Disposition (SPD) project, which aims to dilute and dispose of surplus plutonium oxide. Gamma-ray imagers can be used to determine holdup without interrupting normal operations. In this work, we examine techniques for 3D source localization and mass determination using gamma-ray imagers. Coded-aperture imagers provide excellent source localization within the 2D image plane; however, multiple imagers operating in tandem are necessary to identify source location in 3D space. A Maximum Likelihood Expectation-Maximization (MLEM) method for fitting detector mappings is a powerful tool for accomplishing this task. MLEM allows 3D source localization to be simultaneously constrained using multiple gamma-ray imagers by constructing the basis for the MLEM fit using detector mappings from different detector locations stitched together. Each of these basis points represents a singular response from a source in 3D space and is generated using Monte Carlo simulations of sources placed individually at different locations throughout the imager's field of view. Additionally, implementing knowledge of the physical equipment in the simulations of the glovebox used for the SPD project incorporates attenuation effects that are needed to calculate material holdup.

I. INTRODUCTION

A substantial amount of plutonium oxide will be diluted and disposed as part of the Surplus Plutonium Disposition (SPD) project. Accumulation of nuclear material in handling equipment and gloveboxes during this project is of particular interest for the reasons of material control and accountability, criticality safety, and radiation worker safety. The mass of such material, referred to as holdup, is often determined passively through nondestructive assay techniques. The most common methods of measuring holdup, including the Generalized Geometry Holdup (GGH) method [1] and the In-Situ Object Counting System (ISOCS) technique [2], result in uncertainties that are often difficult to quantify and can be quite large [3].

Holdup measurement uncertainties using these techniques are often due to incorrect assumptions about the geometry and location of radioactive material. Coded-aperture gamma-ray imagers have the ability to locate sources of gamma emitters with excellent angular resolution (e.g. $\sim 5^\circ$ below 450 keV across a $95^\circ \times 95^\circ$ field of view for the H420 [4]). This capability makes imagers particularly useful in a holdup setting where the geometry and lo-

cation of radioactive sources are often unknown. Material geometries can be examined with imagers to reduce systematic uncertainties associated with traditional holdup measurements.

In addition to source geometry, a leading source of uncertainty for source strength measurements is the distance from the source to the detector. With the angular location available from coded-aperture imagers, depth is the only remaining value needed to establish the source location in 3D. Source depth can be inferred through the use of imagers at multiple locations with overlapping fields of view. For an overview of the glovebox system integrated with gamma-ray imagers, see Schmitt *et al.* [5]. Because of the ability to discern both material geometry and 3D location, imagers offer unique functionality as the primary measurement instrument in a holdup setting.

We investigate the use of a Maximum-Likelihood Expectation Maximization (MLEM) algorithm in order to reconstruct source locations in 3D. Simulated responses of imagers in multiple locations with overlapping fields of view are generated using a Geant4 model where a point source is sequentially placed at each voxel in the field of view to create the basis set for the MLEM fit. Data from radioactive sources in a variety of configurations were taken using imagers in multiple locations with overlapping fields of view. These data were used to examine the validity of reconstructing source locations in 3D using an MLEM method. Additionally, source material quantification was investigated with the same method.

II. INSTRUMENTATION

The imager used in this investigation is manufactured by H3D, Inc. It features four position-sensitive CZT crystals as the detector volume and a rank-19, Modified Uniformly Redundant Array (MURA) [6] coded-aperture mask [4]. The CZT detector offers better than 1% energy resolution at 662 keV and has a spectroscopic energy range of 50 keV to 1.5 MeV in coded-aperture mode, although the efficiency falls off at several hundred keV. The detector volume is also sufficiently large ($>$19 cm^3) to allow for compton imaging. This capability extends the angular range of the detector to full 4π at the expense of angular resolution ($\sim 20^\circ$ at > 250 keV).

The mask pattern (shown in Fig. 1) is designed such that a simple cross correlation between the mask pattern and the detector mapping produces a delta function at the angular source location in the imaging plane [7]. Additionally, the mask pattern is antisymmetric about a 90° rotation. This feature allows unmodulated backgrounds to be subtracted effectively while preserving the detector mapping [8]. Nonuniform backgrounds from sources that are not modulated by the coded-aperture mask will produce similar effects in the detector for both mask and antimask data. Therefore, the backgrounds can be accounted for by subtracting antimask data from mask data after normalizing for counting time.

III. SETUP

In order to test methods for 3D reconstruction, radioactive sources were positioned in a variety of configurations using a tripod with an L-shaped source holder (Figure 2) in a plane parallel to the floor. Table I describes the different source configurations used. Images were taken in 10 minute runs (5 minutes each for mask and antimask) for all configurations at 22.5° increments in a semi-circle centered at the base of the tripod.

^{133}Ba was chosen for the source material because of its prominent lines at about 81 and

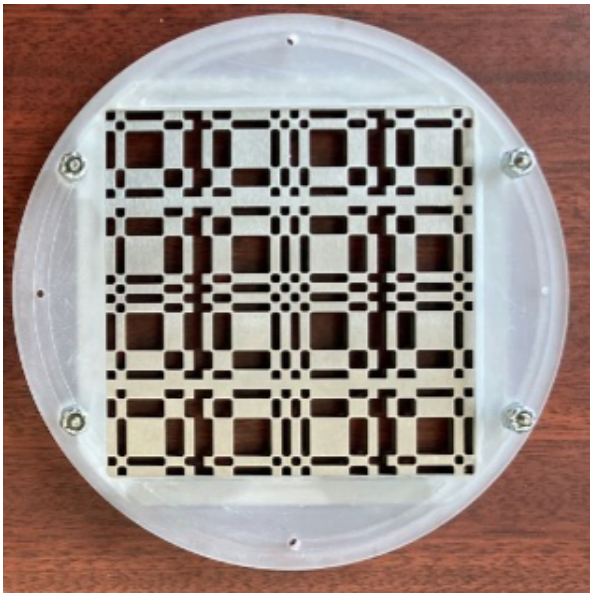

FIG. 1. MURA coded-aperture mask made of tungsten used to attenuate gamma-rays and produce a shadowgram on the position-sensitive detector.

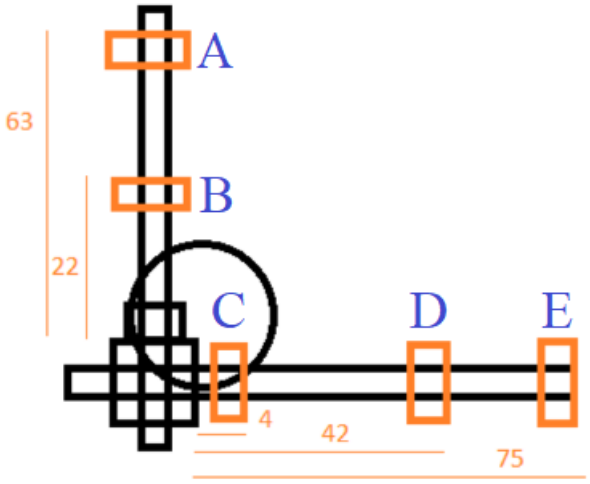

FIG. 2. Blacks lines detail the source holder, orange boxes represent potential source locations denoted by blue letters, and distances from center are given in centimeters.

356 keV. The analysis here was performed using the 81 keV gamma ray. Using a low energy gamma ray minimizes the need for depth corrections and compton scattering in the detector and ensures optimal attenuation of the gamma rays by the tungsten coded-aperture mask. Two different source strengths were chosen to examine the dynamic range of the imager system, namely the ability to identify and locate weak sources in the field of a stronger source. The strong source was nominally 400 µCi while the two weaker sources were an order of magnitude lower at 40 µCi each. Investigations into the dynamic range using these combinations of strong and weak sources are the subject of future efforts. For this work, only data sets containing the strong source alone were used.

TABLE I. Source locations for each configuration. S denotes the strong (∼400 µCi) source while R and L denote the weak (∼40 µCi) sources.

Configuration	A	B	C	D	E
1			S		
2				S	
3					S
4		R	S	L	
5	R		S	L	
6	R		S		L
7		R		L	
8	R				L

IV. ANALYSIS METHOD

Fundamentally, the imager data for an unknown number and location of sources can be thought of as a linear combination of point sources in a voxelized 3D space. In order to reconstruct source locations and determine their strengths, the imager response to point sources in each voxel are simulated in Geant4. These simulations form the basis set for an MLEM fit to the data. The MLEM method used in this analysis is based on Bayes' Theorem which relates causes and effects probabilistically. The derivation of the iterative formula is described by Tain and Cano-Ott in section 3.3 of Ref. [9]. This formula ensures positivity of the solution which is required for physically relevant results. Since the relation of the individual basis points is linear, uncertainties are calculated simply by propagation of errors.

Since the MLEM algorithm described above requires non-negative bin values, the fit is executed on raw detector mappings without performing the usual cross correlation that provides an image. Additionally, the mask minus antimask method for subtracting unmodulated backgrounds is not feasible. To account for these backgrounds, mask and antimask data are stitched together as one histogram and fit simultaneously. An example of this data arrangement is shown in Figure 3. Since unmodulated backgrounds produce similar pixel-by-pixel responses in both mask and antimask data, they can be modeled by ad hoc response functions containing an equal number of counts in a single pixel for both mask and antimask. One of these response functions is included for each detector pixel. This technique was developed by Brubaker *et al.* [10].

In order to assess the validity of this approach, a nonuniform, unmodulated background was arbitrarily added to the detector response of a simulated point source and fit with the MLEM method. The results of this fit are shown in Figure 4. This result demonstrates that including an ad hoc response function for each detector pixel that contains an equal number of counts in the mask and antimask response can appropriately model the presence of a nonuniform, unmodulated background.

With "true signals" and backgrounds effectively isolated, localization in 3D space is the next objective from our analysis method. This is accomplished by incorporating data from imagers taken at multiple locations with overlapping fields of view. The detector mappings for a mask and antimask pair for each detector view are normalized for counting time and stitched together to form a single histogram. The same is done with the simulated response functions that form the basis set for the MLEM fit. Each response function in the basis

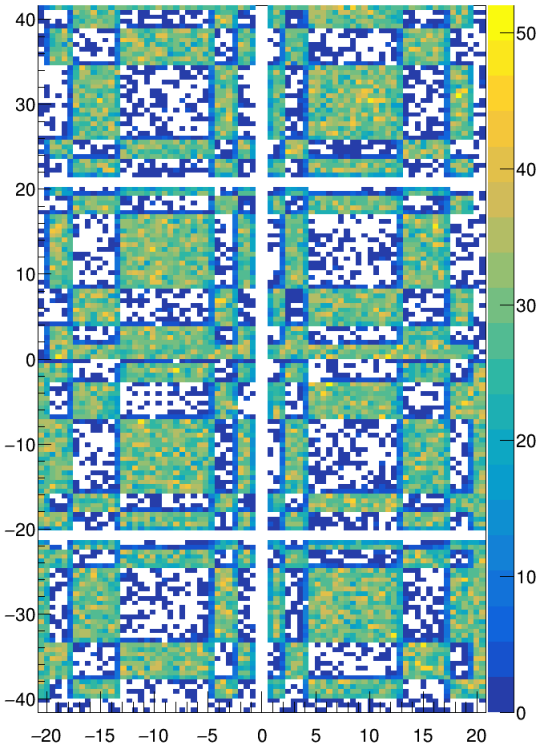

FIG. 3. Mask (top) and antimask (bottom) detector mappings from a simulated point source in the center of the field of view. Note that open holes in the mask response are inverted to closed pixels in the antimask response and vice versa.

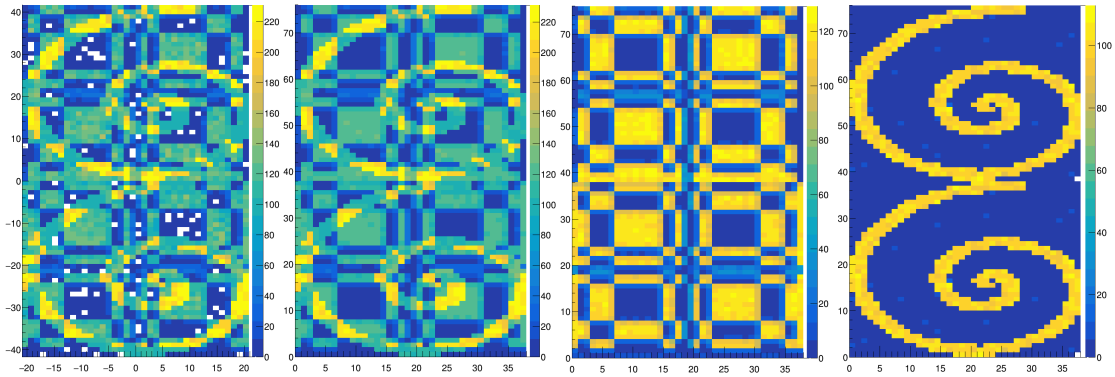

FIG. 4. From left to right, simulated detector response with an arbitrary and nonuniform unmodulated background added in post-facto, the MLEM total fit result including the ad hoc single pixel response functions, the portion of the fit from only simulated sources representing the "true signal", and the ad hoc response functions representing the unmodulated background.

set is the response of the entire detector array (in this case 2 detectors) to a single point source in 3D space. An example of such a response function is shown in Figure 5. Fitting the experimental data taken by a system of two detectors with an MLEM algorithm using the 2-detector simulated responses to point sources in a voxelized space allows 3D source locations and strengths to be determined.

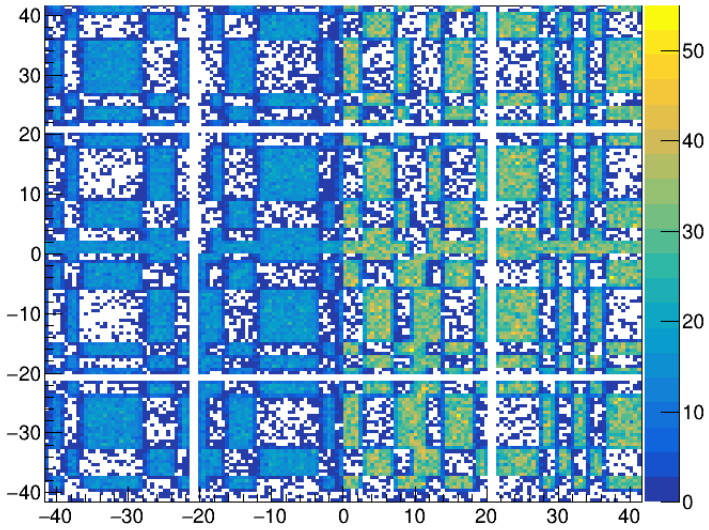

FIG. 5. Mask (top) and antimask (bottom) simulated responses for a 0 degree (left) detector and 45 degree (right) detector. In this case, the simulated source is closer to the 45 degree detector, hence the higher count rate in its side of the response.

V. RESULTS

Since the signal and the background can be separated and sources can be located in 3D space using multiple angles, it is straightforward to deduce source strengths from the simulated source activity and the scale factor determined by the MLEM fit to the data. This method will be particularly powerful for making a quantitative measurement in a holdup setting where there is prior knowledge of equipment in the measurement setting. If such equipment is included in the simulation of the basis set for the fit, then important corrections like attenuation through objects are "baked in" to the simulation.

The basis set of simulated detector response functions was first chosen to be a 21x21x7 box of evenly-spaced point sources spanning the 160x160x12 cm^3 voxelized space containing the experimental sources. A top-down, 2D projection in the plane of the source holder of the fit results for configuration 1 (a single, strong source near the center of the source holder) are shown in Figure 6. The result of this fit localizes the source approximately 9 cm away from the expected location and provides an activity measurement of 532 µCi. The fit for configuration 3 (strong source at the end of one arm of the source holder) provides slightly different results, this time the source is found 17 cm away from the expected source location and a source strength of 534 µCi. The 2D projection for this fit is shown in Figure 7.

To investigate the ability of the algorithm to find and quantify multiple sources, the previous two data sets were added together, normalized for counting time, and fit with the algorithm. Results of this fit are shown in Figure 8. The algorithm now places the distant source (near the center of the holder) about 13 cm from the expected location. The activity measurement also shows greater disagreement as it is measured to be ∼640 µCi. The near source (at the end of one source holder arm) is found about 18 cm from its expected location and is measured to be ∼538 µCi.

To improve source localization (and thus strength measurement), the simulated basis set may be regularized to the physical system of interest. In this case, it is known *a priori* that

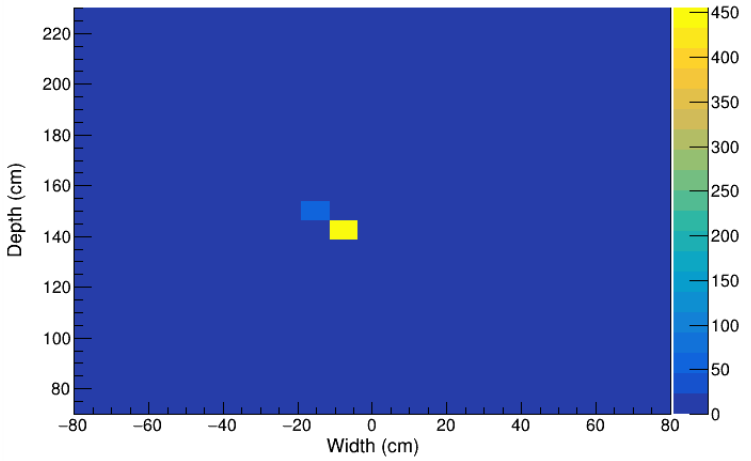

FIG. 6. Top-down 2D projection of 3D fit results for configuration 1.

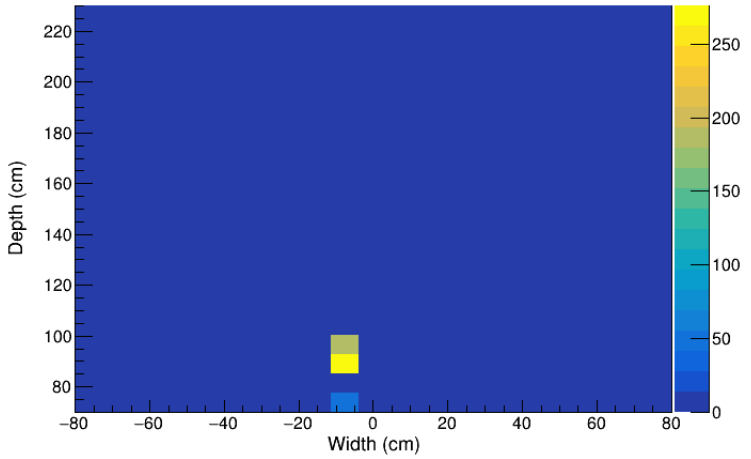

FIG. 7. Top-down 2D projection of 3D fit results for configuration 3.

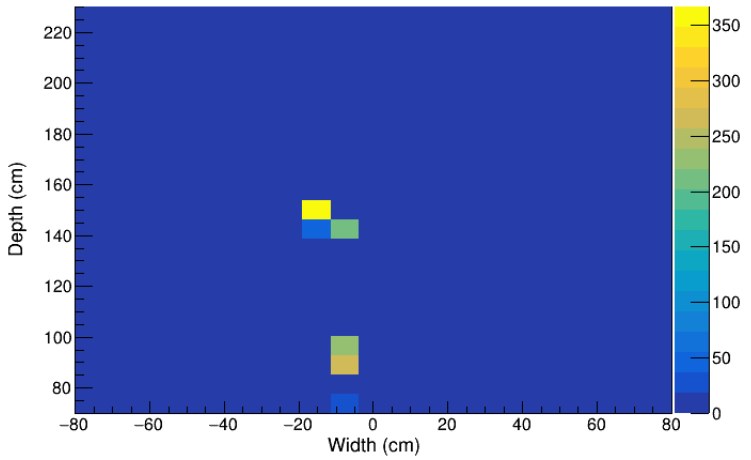

FIG. 8. Top-down 2D projection of 3D fit results for a combination of configuration 1 and 3 normalized by counting time.

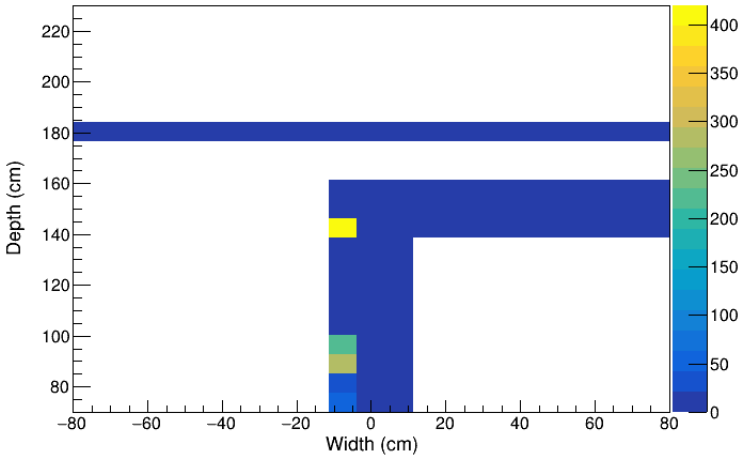

FIG. 9. 2D projection of 3D fit results for a combination of configuration 1 and 3 normalized by counting time. The basis set for this fit has been regularized using *a priori* knowledge of the physical system.

sources must lie along the arms of the source holder and cannot originate from thin air, so it is reasonable to include only response functions that have point sources near these locations in the fit. In the interest of future application to a glovebox setting, a wall of point sources behind the source holder are also included to represent the floor of a glovebox. The results of this fit for the two-source configuration are shown in Figure 9.

This regularization provides the source location of the far source to within 9 cm of the known source location and measures the activity as 419 µCi. The location identified for the close source is less precise and is approximately 17 cm further from the detectors than the expected source location. As a result, the measured activity is about 590 µCi.

VI. DISCUSSION

One observation from these results is that sources are more accurately located when they are near the intersection of the lines of sight of the imagers. In this instance, the imagers are oriented at a 45° angle from one another and both are pointed to the center of the source holder about 150 cm away. One potential cause of the mismatch between fit location and reality is an incorrect assumption about the position and/or orientation of the imagers. Since the simulated basis set is constructed by assuming an ideal position and orientation of each detector, a significant deviation from this ideal case (e.g. one imager positioned lower or oriented with an unplanned tilt in the line of sight) will cause the basis points to not be representative of the data taken with the physical system. It is possible for the suitability of response functions to vary across the reconstructed volume depending on the source of the deviation from the ideal. More work will have to be done to assess whether this is a viable explanation for misplaced sources in this work.

Another phenomenon apparent from these results is that measured activities are not consistent with known values after accounting for incorrect 3D position reconstruction. Because of the inverse square law, sources that are further away must be stronger sources to produce the same count rate as closer sources. Therefore, sources that are inaccurately determined to be further from the detector array than they actually are will be reconstructed to be

stronger than their actual activity level. This is not always what we see in this experiment. A correction can be applied to the known source activity (400 µCi) based on the incorrectly identified source location for each configuration and fit result. This helps determine if the deviation from expected source strength is due entirely to inaccurate source locations or if there is some other systematic error. Table II shows a comparison of the expected measured source strength accounting for the incorrectly identified location to the source strength determined by the fit.

TABLE II. MLEM fit results for a variety of configurations compared to the distance-corrected, expected activity.

Configuration	Expected Distance to 0° Det (cm)	Reconstructed Distance to 0° Det (cm)	Distance-Corrected Expected Activity (µCi)	Reconstructed Activity (µCi)
1	146	144	387	532
3	75	91	583	534
1 + 3 (Far)	146	147	407	640
1 + 3 (Near)	75	92	597	538
1 + 3 (Regularized, Far)	146	142	381	419
1 + 3 (Regularized, Near)	75	90	576	590

A potential underlying cause for each of these issues is simply a disagreement between the detector data and the simulations. Current comparisons of the imager's intrinsic efficiency to the efficiency of the simulated detector reveal key discrepancies. Much work is currently being done to identify the source of these discrepancies and rectify them in the simulations. For a summary of the current state of these models, see Ref. [11]. Specifically, the intrinsic efficiency of the imager varies differently as a function of source location compared to simulation. The simulated response function for a source that lies in different regions of the field of view for each imager will not accurately model the difference in detected source intensity since the efficiency of the detector is not modeled correctly. This will cause both a spatial and source strength blurring as the MLEM algorithm attempts to reconstruct experimental data using a basis set that does not include the true solution.

VII. CONCLUSIONS

An MLEM method for deconvolving data from a system of gamma-ray imagers was investigated as a means to locate and quantify sources in 3D. The theoretical basis for the algorithm is treating the data as a linear combination of detector responses to point sources in space (the basis set) and solving the inverse problem iteratively. The basis set is

constructed by simulating the detector responses to point sources in space using a Geant4 model. A particular strength of this method is that common nondestructive assay correction factors such as attenuation through objects will be "baked in" to any physical simulation of the basis set. To date, the algorithm has been shown to locate single sources within ∼25% of the expected source location and determine source strengths within ∼33% of expected source strengths. Both of these performance metrics are expected to improve with a more detailed basis set and more physically representative simulated detector responses. Future work will determine the source of the systematically high activity measurements as well as quantify the uncertainty of mass measurements in a holdup setting.

---

[1] P. A. Russo, Gamma-ray measurements of holdup plant-wide: application guide for portable, generalized approach, LA-14206 (2005).

[2] V. Nizhnik, A. Belian, A. Shephard, and A. Lebrun, In situ object counting system (ISOCS™) technique: A cost-effective tool for NDA verification in IAEA safeguards, in *2011 2nd International Conference on Advancements in Nuclear Instrumentation, Measurement Methods and their Applications* (2011) pp. 1–5.

[3] A. Lousteau and J. Stooksbury, Comparison of holdup detection systems, (2012).

[4] H420—gamma-ray imaging spectrometer, `https://h3dgamma.com/H420Specs.pdf`, accessed: 2023-04-6.

[5] K. Schmidt, Implementation of a system of gamma imagers for measuring plutonium holdup, This Proceedings (2023).

[6] S. R. Gottesman and E. E. Fenimore, New family of binary arrays for coded aperture imaging, Appl. Opt. **28**, 4344 (1989).

[7] E. E. Fenimore and T. M. Cannon, Coded aperture imaging with uniformly redundant arrays, Appl. Opt. **17**, 337 (1978).

[8] J. Braga, T. Villela, U. Jayanthi, F. D'Amico, and J. Neri, A new mask-antimask coded-aperture telescope for hard X-ray astronomy, Experimental astronomy **2**, 101 (1991).

[9] J. Tain and D. Cano-Ott, Algorithms for the analysis of β-decay total absorption spectra, Nuclear Instruments and Methods in Physics Research Section A: Accelerators, Spectrometers, Detectors and Associated Equipment **571**, 728 (2007).

[10] E. M. Brubaker, A maximum likelihood expectation maximization iterative image reconstruction technique for mask/anti-mask coded aperture data, in *2013 IEEE Nuclear Science Symposium and Medical Imaging Conference (2013 NSS/MIC)* (2013) pp. 1–3.

[11] K. Ziock, Efficiency calibration of the h3d h420 gamma-ray imager, This Proceedings (2023).